LETTERS

Force-induced activation of covalent bonds in mechanoresponsive polymeric materials

Douglas A. Davis[1], Andrew Hamilton[2], Jinglei Yang[3]†, Lee D. Cremar[1], Dara Van Gough[4], Stephanie L. Potisek[1], Mitchell T. Ong[1], Paul V. Braun[1,3,4], Todd J. Martínez[1,3]†, Scott R. White[3,5], Jeffrey S. Moore[1,3,4] & Nancy R. Sottos[3,4]

Mechanochemical transduction enables an extraordinary range of physiological processes such as the sense of touch, hearing, balance, muscle contraction, and the growth and remodelling of tissue and bone[1–6]. Although biology is replete with materials systems that actively and functionally respond to mechanical stimuli, the default mechanochemical reaction of bulk polymers to large external stress is the unselective scission of covalent bonds, resulting in damage or failure[7]. An alternative to this degradation process is the rational molecular design of synthetic materials such that mechanical stress favourably alters material properties. A few mechanosensitive polymers with this property have been developed[8–14]; but their active response is mediated through non-covalent processes, which may limit the extent to which properties can be modified and the long-term stability in structural materials. Previously, we have shown with dissolved polymer strands incorporating mechanically sensitive chemical groups—so-called mechanophores—that the directional nature of mechanical forces can selectively break and re-form covalent bonds[15,16]. We now demonstrate that such force-induced covalent-bond activation can also be realized with mechanophore-linked elastomeric and glassy polymers, by using a mechanophore that changes colour as it undergoes a reversible electrocyclic ring-opening reaction under tensile stress and thus allows us to directly and locally visualize the mechanochemical reaction. We find that pronounced changes in colour and fluorescence emerge with the accumulation of plastic deformation, indicating that in these polymeric materials the transduction of mechanical force into the ring-opening reaction is an activated process. We anticipate that force activation of covalent bonds can serve as a general strategy for the development of new mechanophore building blocks that impart polymeric materials with desirable functionalities ranging from damage sensing to fully regenerative self-healing.

We created mechanoresponsive synthetic polymeric materials by directly linking force-activated mechanophores into the polymer chains of bulk polymers or by using the mechanophores as cross-links (Fig. 1). The mechanophore motif must efficiently transfer external force to a relatively small number of specific bonds in the bulk polymer, with this mechanochemical activation depending critically on the molecular structure of the mechanophore and the attachment points to the polymer chains. To demonstrate directly that external forces can locally activate a mechanophore linked into elastomeric or glassy polymer solids, we first selected a mechanophore with the potential to undergo a force-induced, 6-π electrocyclic ring-opening reaction[17] that is accompanied by a colour change (Fig. 1a). The selected molecule is well-characterized and exhibits both thermo- and photochromic responses[18] that reversibly transform a closed, colourless spiropyran form to a highly coloured, planar merocyanine structure through rupture of the spiro carbon-oxygen (C–O) bond. The increased conjugation of the merocyanine form shifts the absorption to longer wavelengths, thus giving rise to visible colour and fluorescence. The spiro C–O bond is the critical point for mechanically induced activation, and there are many possible attachment points on the spiropyran that differ in their ability to transmit force efficiently across the junction (Fig. 1a). Simple mechanical models indicate that attachment on opposing sides of the spiro-junction, specifically positions 5′ or 6′ of the indole side and positions 7 or 8 of the benzopyran side, preferentially stresses the spiro C–O bond over the spiro C–C bond.

We selected positions 5′ and 8 as the attachment points and functionalized them with α-bromo or methacryloyl esters for subsequent polymerization by single-electron-transfer living radical polymerization[19] or suspension radical polymerization, respectively (Fig. 1b, structures **1** and **4**). We prepared control structures to determine whether the observed colour change was dependent on linking through the spiro-junction or was the result of other factors, such as localized heating or radical generation from polymer chain cleavage during mechanical deformation[20]. The monofunctional control lacked the polymer chain attached to the indole portion (Fig. 1c, structures **2** and **5**), precluding the transfer of any substantial force into the spiropyran. A difunctional control (Fig. 1c, structure **3**) with a structure closer to the purported mechanophore was prepared by placing the spiropyran in the centre of the polymer chain, but with polymer chains linked only to one side of the spiro-junction. This placement allowed the transfer of force to the spiropyran, but not to the spiro-fused C–O bond specifically.

We modelled the effect of external force on the mechanophore (Fig. 2a) with both first-principles steered molecular dynamics[21–23] and constrained optimization (COGEF)[24] simulations, and using truncated (**t**) as well as extended (**e**) models of the mechanophore unit **1** (insets to Fig. 2c and d, see also Supplementary Figs S6 and S7). The results of dynamics simulations using density functional theory (DFT) are shown in Fig. 2b for mechanophore model **1t** and difunctional control model **3t**. The C–O distance at the spiro bond is plotted as a function of time for a variety of applied forces, ranging from 2 to 3 nN. For **1t**, scission occurred exclusively at the C–O bond for all applied forces investigated within this range (Supplementary Video S2). For **3t**, no C–O bond rupture was observed on the indicated timescale (Supplementary Video S3).

The origin of this behaviour was further explored using the COGEF procedure at the DFT level (Fig. 2c). For **1t**, the potential energy of the molecule rose as the distance between the attachment points increased, leading to a reaction activation barrier of 2.3 eV at an

[1]Department of Chemistry, [2]Department of Mechanical Science and Engineering, [3]The Beckman Institute, [4]Department of Materials Science and Engineering, [5]Department of Aerospace Engineering, University of Illinois at Urbana-Champaign, Illinois 61801, USA. †Present addresses: School of Mechanical and Aerospace Engineering, Nanyang Technological University, Singapore (J.Y.); Department of Chemistry, Stanford University, Stanford, California, USA (T.J.M.).

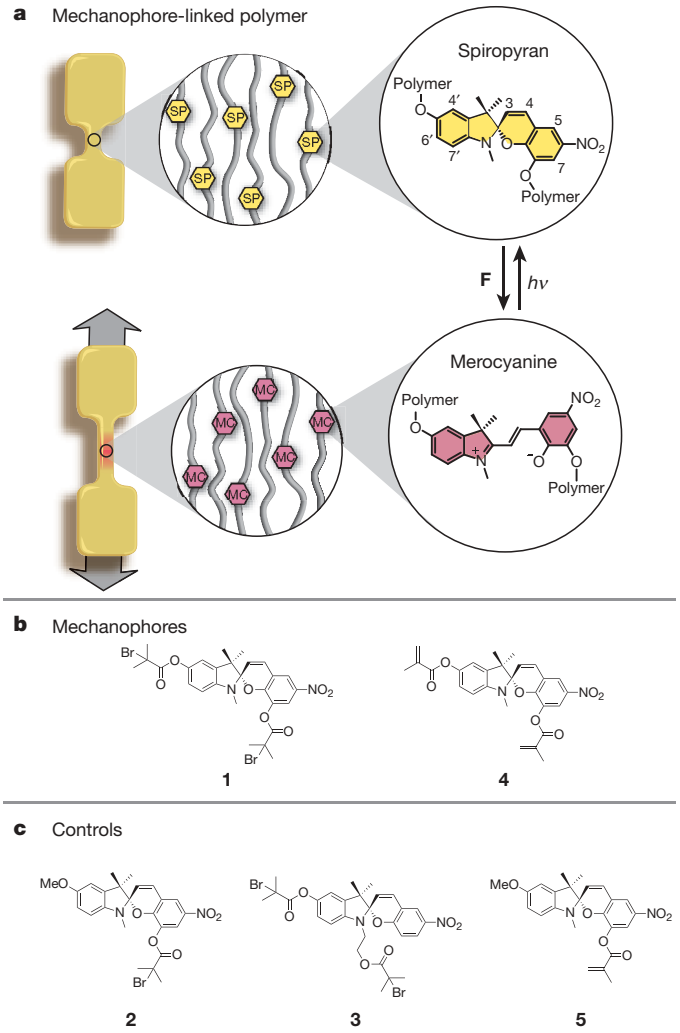

Figure 1 | Chemical structures and bulk polymeric samples. a, Schematic diagram of 'dog bone' specimens prepared from linear 80 kDa PMA. Upon application of tensile force, a hypothesized conversion between the colourless spiropyran and coloured merocyanine forms of the mechanophore occurs. Exposure to visible light reverses the conversion back to the original spiropyran form. **b**, The polymer connectivity of spiropyrans **1** and **4** is across the spiro-junction, and therefore these materials are expected to be mechanically active. **c**, Materials derived from spiropyrans **2**, **3** and **5** serve as controls, since the polymer connectivity does not include the spiro-junction. Spiropyrans functionalized with α-bromo esters were used to initiate single-electron-transfer living radical polymerization and incorporate a single spiropyran in the middle (**1**, **3**) or at the end (**2**) of the polymer chain. Spiropyrans functionalized with methacryloyl esters (**4**, **5**) were copolymerized with methyl methacrylate in aqueous suspension to form PMMA beads incorporating spiropyrans at cross-linked junctions (**4**) or as pendant groups (**5**).

elongation of 17%; further elongation of the molecule to 20% ruptured the spiro C–O bond. In contrast, **3t** showed no C–O bond rupture at 20% elongation and the activation barrier increased to 3.7 eV at an elongation of 24%; further elongation finally caused rupture of the N–H bond. In the case of the extended models, the DFT COGEF energy profiles for **1e** (Fig. 2d) again showed spiro C–O bond rupture, whereas the difunctional control molecule **3e** underwent a bond rupture at one of the side chains that does not lead to a colour change. Rupture of this side chain required more energy than that needed to activate **1e**. Thus, the COGEF calculations predicted selective spiro C–O bond rupture for the **1t** as well as the **1e** models. Semi-empirical calculations were in good agreement with DFT for both the truncated and extended models (Supplementary Figs S9 and S12), justifying their use in longer-lasting dynamics simulations to explore the effects of lower applied forces.

Experimentally, mechanochemical transduction was demonstrated for an elastomeric mechanophore-linked poly(methyl acrylate) (PMA) and a glassy mechanophore cross-linked poly(methyl methacrylate) (PMMA). Elastomeric materials consisted of **1**, **2** or **3** polymerized into PMA, resulting in a single mechanophore per chain. Polymer samples were heat moulded into a 'dog bone' shape, which was loaded either monotonically or cyclically under displacement control while monitoring the applied stress (Fig. 3a). Glassy materials consisted of solutions of **4** and **5** in a methyl methacrylate suspension copolymerized using benzoyl peroxide and *N*,*N*-dimethylaniline to give 100–500 μm diameter beads (Fig. 4a). These PMMA beads were compressed with a stepper actuator coupled to a load cell, which allowed for strain rate control while monitoring the resulting stress.

The active mechanophore-linked PMA (PMA-**1**-PMA), the monofunctional control (PMA-**2**), and the difunctional control (PMA-**3**-PMA) specimens were tested to failure under monotonic tensile loading. An intense colour change occurred in the active specimen (the absorption band is in the 550–590 nm range; Supplementary

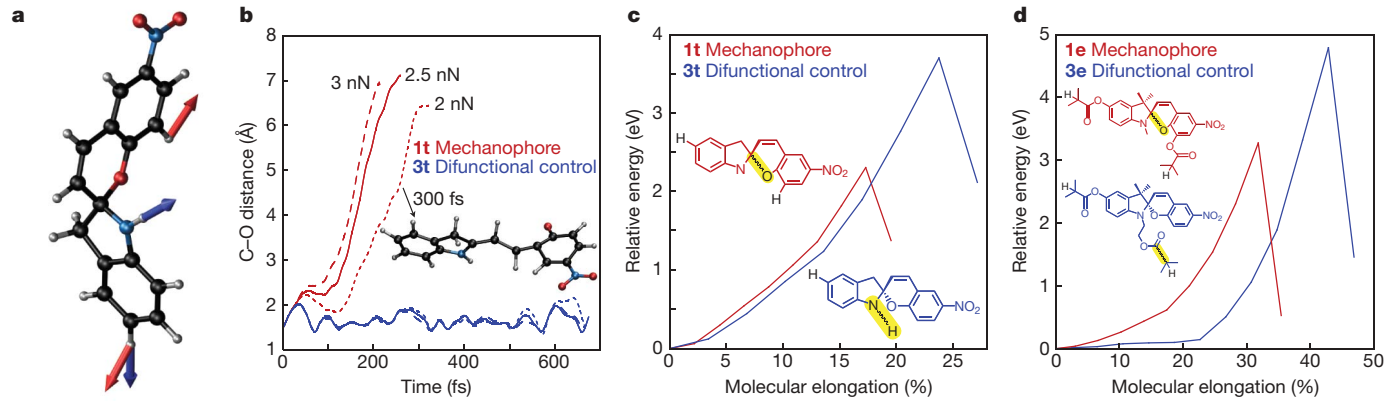

Figure 2 | First-principles dynamics and constrained optimization models of mechanical activation. a, Truncated model of spiropyran showing the pulling directions (mechanophore **1t**, red arrows; control **3t**, blue arrows). The extended model includes ester chains in place of the H atoms (see inset of **d**). **b**, Steered molecular dynamics for the truncated mechanophore and control. The C–O bond distance is plotted versus time at 2, 2.5 and 3 nN, as shown. **c**, Potential energy versus percentage elongation for the truncated models (**1t** and **3t**) calculated at the DFT level. Elongation, the distance between the pulled H atoms, is increased systematically and all other geometric coordinates are optimized at each point. Bond rupture occurs at the highlighted spiro C–O and N–H bonds for **1t** and **3t**, respectively. **d**, Potential energy for the extended models (**1e** and **3e**) calculated with DFT. Elongation is the distance between the terminal H (instead of Br in **1** and **3**) atoms on the side chains. Rupture for **1e** and **3e** occurs at the highlighted C–O spiro and C–C ester bonds, respectively.

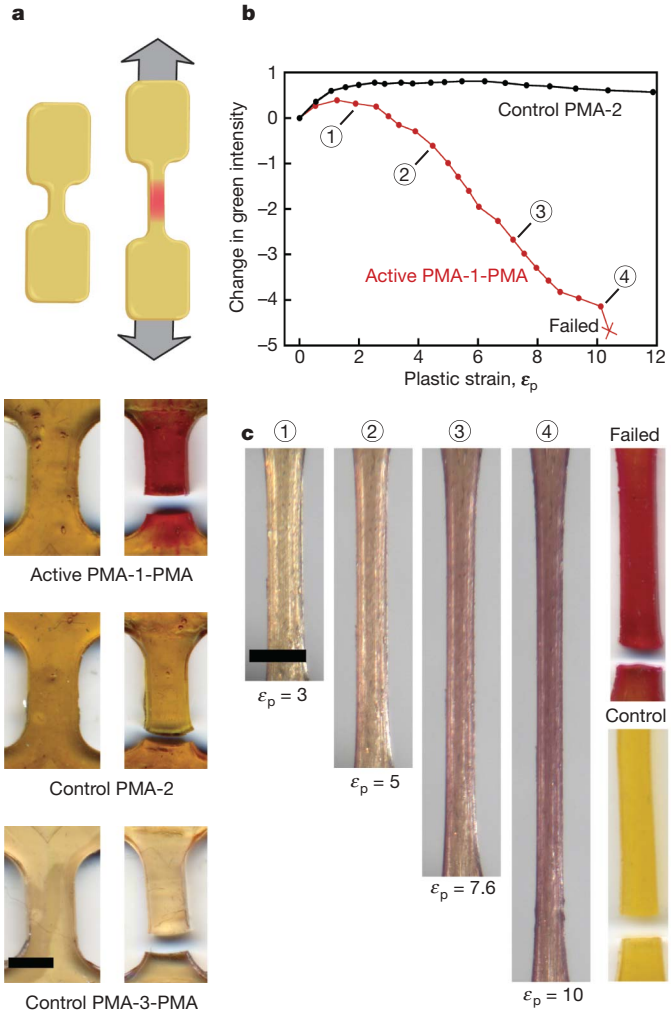

Figure 3 | Mechanochromic response of mechanophore-linked PMA elastomer under tensile loading. **a**, Schematic of tensile loading direction. Optical images of active PMA-**1**-PMA, monofunctional control PMA-**2**, and difunctional control PMA-**3**-PMA specimens before testing and after failure in monotonic tension. **b**, Accumulation of plastic (unrecovered) strain and relative change in green intensity for active PMA-**1**-PMA and monofunctional PMA-**2** control samples after each loading cycle in a fatigue test. **c**, Optical images of an active PMA-**1**-PMA specimen acquired after the loading cycles indicated in **b** and just after failure. For comparison, a failed monofunctional PMA-**2** control sample subjected to the same cyclic loading regimen is included (lower right). Scale bars in **a** and **c** are 2 mm.

Fig. S17), whereas no colour change was observed in the monofunctional or difunctional controls (Fig. 3a). The mechanically induced colour change could be reversed after approximately 6 h of exposure to fluorescent room light.

We further evaluated the evolution of the colour change in the active PMA-**1**-PMA by a cyclic loading regime, in which increasing levels of strain were applied with each cycle (Supplementary Figs S3 and S4) causing plastic (unrecovered) strain to accumulate during the testing time frame. Digital images of the gauge section were acquired after each cycle, and the change in the RGB (red, green, blue) colour ratios was analysed as described in Supplementary Fig. S14.

The representative images of the active PMA-**1**-PMA samples undergoing cyclic loading in Fig. 3c reveal the emergence of red colour with increasing plastic deformation. The corresponding relative change in the green channel intensity is plotted in Fig. 3b as a function of the accumulated strain at the end of each loading cycle. The active PMA-**1**-PMA shows a nearly monotonic reduction in the relative green intensity after reaching a plastic strain level of 200%. In contrast, the monofunctional control PMA-**2** exhibited no change in the green intensity level throughout the loading regime. After reaching a strain level of just over 1,000%, the active PMA-**1**-PMA failed, leaving an intense red colour throughout the entire gauge section. An image of the failed monofunctional control PMA-**2** sample is also included in Fig. 3c for comparison. The lack of activation in the control samples provides strong evidence that the colour change is induced solely by the application of mechanical force, rather than by temperature change or photolytic activation (Supplementary Table S1).

We adapted a compressive loading configuration (Fig. 4a) for the glassy, mechanophore cross-linked PMMA-**4** and corresponding monofunctional PMMA-**5** control beads. Although compressive stresses (σ_1) develop in the bead parallel to the loading direction (X_1), significant tensile stresses (σ_2) are induced perpendicular to the loading direction (X_2). Elastic predictions[25,26] of the σ_2 stress field on the equatorial plane of a compressed bead are plotted along the X_2 axis in Fig. 4b, and a more detailed stress analysis is included in the Supplementary Information. The maximum tensile stress develops in the centre of the bead ($r = 0$) and reaches a value of 0.6 of the magnitude of the applied compressive stress (σ_o). Hence, compressive loading generates tensile stresses that are expected to activate mechanophore **4** in this configuration. For this specimen geometry, we characterized mechanochemical activation by analysis of the relative change in RGB intensity during loading (Supplementary Video S7) and the relative change in fluorescence after testing.

The evolution of a mechanochemically induced colour change in the active cross-linked PMMA-**4** bead is shown in Fig. 4a and c for a representative compression test. The colour change emerges in the centre of the bead at a strain level just beyond the yield point. The corresponding fluorescence intensity, as measured by confocal laser scanning microscopy, is plotted across the equatorial plane in Fig. 4b. The maximum fluorescence intensity at the bead centre correlates with the predicted tensile stress distribution (just before yield) in the same plane. No detectable change in colour or significant fluorescence was observed for the monofunctional control PMMA-**5** beads (Supplementary Fig. S18). As with the mechanophore-linked PMA, the evolution of colour in the active cross-linked bead corresponds to a reduction of the relative green channel intensity, and the colour (and fluorescence) intensifies with accumulation of plastic strain. The colour change in the glassy PMMA is more stable than in PMA and remains after several weeks of exposure to fluorescent room light.

To explore further the relationship of colour change with the onset of yielding, we characterized the threshold stress and strain levels required to produce colour change in the active cross-linked PMMA-**4** beads over a range of strain rates. As shown in Fig. 4d, the yield stress and threshold stress both increased linearly with the natural log of the strain rate, while the threshold strain remained nearly constant. This relationship between threshold stress, yield stress and strain rate indicates that the mechanochemical reaction in the bulk polymer may be a strain-activated rate process[27]. With plastic flow above a strain threshold, activation of the mechanophore-linked polymer is achieved, and a colour signature is obtained.

We have shown that routinely encountered loads and strain rates are sufficient to trigger covalent bond changes with appropriately designed mechanophores. The spiropyran mechanophore can function as a molecular force sensor, providing visible detection and mapping of mechanical stresses within bulk polymeric materials. We expect that the spiropyran mechanophore will serve as a molecular probe to aid in understanding the effects of stress and damage on polymeric materials, providing an opportunity for assessment, modification and improvement before catastrophic failure. Overall, the mechanophore motif is general and capable of translating many other desirable responses including polymerization, cross-linking or even strain-activated mechanical fuses. With a deeper understanding of mechanophore design and efficient chemical response pathways, we envision new classes of dynamically responsive polymers that locally remodel, reorganize or even regenerate upon mechanical stimulation.

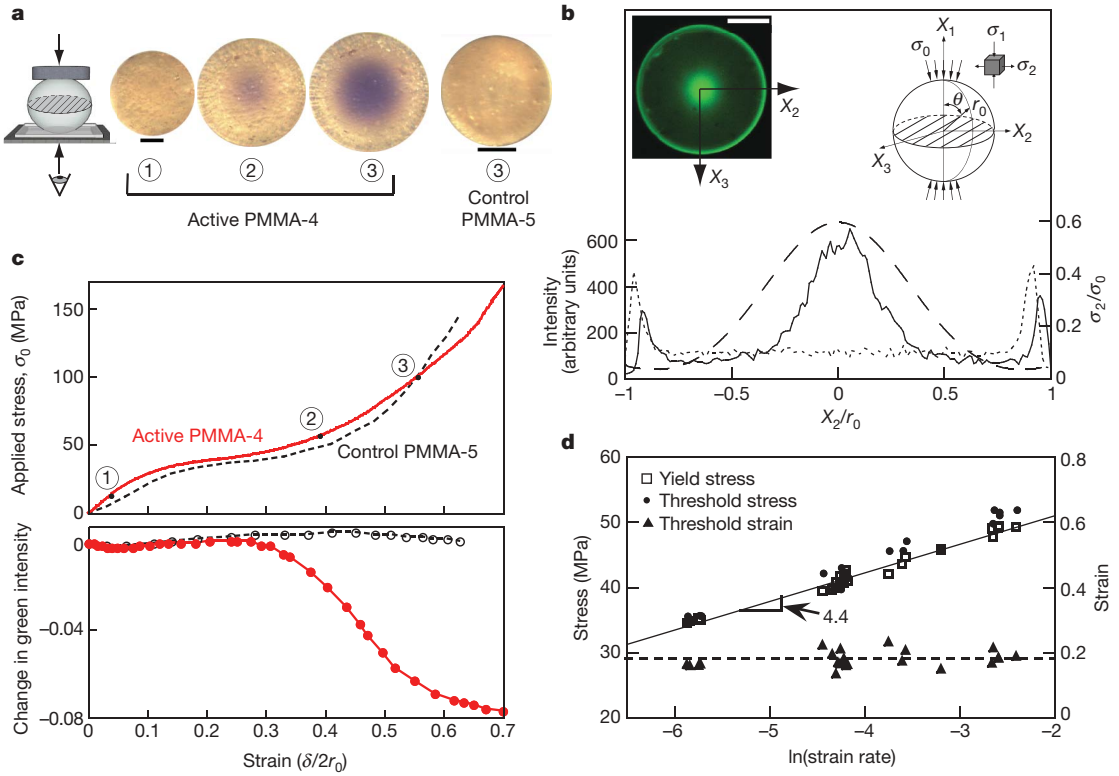

Figure 4 | Mechanochromic response of glassy mechanophore cross-linked PMMA beads under diametral compression. **a**, Schematic of compression loading; deformed beads are imaged from bottom. Optical images as indicated on the stress–strain curve in **c**. Scale bars 50 μm. **b**, Measured fluorescence intensity in the equatorial plane for a bead deformed just past the yield point (left inset, scale bar 50 μm). Initial signature (dotted line) and fluorescence intensity after deformation (solid line) plotted along the X_2 axis. Elastic prediction (dashed line) of the normalized transverse stress field, σ_2/σ_0 ($\sigma_0 = P/\pi r_0^2$) for a bead subject to uniformly distributed compression load (right inset). **c**, Compressive stress (σ_o) and relative change in green intensity as a function of applied compressive strain for the active difunctional PMMA-**4** (red line and red dots) and monofunctional control PMMA-**5** (black line and black dots) beads. **d**, Threshold (colour) stress and yield stress are nearly coincident as a function of strain rate, while the threshold strain remains relatively constant.

METHODS SUMMARY

Materials. The spiropyran functionalized PMA was compression moulded into non-standard 'dog bone' shaped tensile samples (Supplementary Fig. S1). The PMA material was pressed in an aluminium mould at 54 °C under 100 pounds per square inch (psi) for five minutes, and then cooled to room temperature while holding the pressure at 100 psi. Any thermally induced ring-opening of the mechanophore during processing was reversed by illumination with intense white light. Mechanophore cross-linked PMMA beads were annealed at 90 °C and illuminated with bright visible light for 2.5 h to close the merocyanine to the spiropyran form.

Mechanical testing. PMA samples were tested on a screw-driven load frame. The initial gauge length ranged between 2 and 4 mm. For monotonic tension tests, samples were loaded under displacement control at a rate of 1.5 mm s^{-1} to failure. For fatigue tests, the sample was initially loaded to a maximum extension of twice the gauge length and then unloaded. The maximum extension of subsequent loading cycles was increased by the initial gauge length each time, such that on the second cycle the maximum extension was three times the initial gauge, on the third cycle it was four times the initial gauge length, and so on until the sample failed. Compression tests of spiropyran functionalized PMMA beads were conducted using a custom-built apparatus (Supplementary Fig. S5) at loading rates ranging from 1 to 25 μm s^{-1}. The beads were immersed and tested in oil with a refractive index (1.518) similar to that of PMMA (1.50) to minimize light scattering and improve imaging. A confocal scanning laser microscope (Leica SP2) in fluorescence mode exciting with 543 nm laser light and collecting between 570 and 650 nm was used to obtain fluorescence images.

More detailed descriptions of the materials synthesis and mechanical test protocols are provided in the Supplementary Information.

Received 12 November 2008; accepted 5 March 2009.

1. French, A. S. Mechanotransduction. *Annu. Rev. Physiol.* **54,** 135–152 (1992).
2. Orr, A. W., Helmke, B. P., Blackman, B. R. & Schwartz, M. A. Mechanisms of mechanotransduction. *Dev. Cell* **10,** 11–20 (2006).
3. Gillespie, P. G. & Walker, R. G. Molecular basis of mechanosensory transduction. *Nature* **413,** 194–202 (2001).
4. Lele, T. P., Thodeti, C. K. & Ingber, D. E. Force meets chemistry: Analysis of mechanochemical conversion in focal adhesions using fluorescence recovery after photobleaching. *J. Cell. Biochem.* **97,** 1175–1183 (2006).
5. Mahadevan, L. & Matsudaira, P. Motility powered by supramolecular springs and ratchets. *Science* **288,** 95–99 (2000).
6. Martinac, B. Mechanosensitive ion channels: molecules of mechanotransduction. *J. Cell Sci.* **117,** 2449–2460 (2004).
7. Beyer, M. K. & Clausen-Schaumann, H. Mechanochemistry: The mechanical activation of covalent bonds. *Chem. Rev.* **105,** 2921–2948 (2005).
8. Löwe, C. & Weder, C. Oligo(*p*-phenylene vinylene) excimers as molecular probes: deformation-induced color changes in photoluminescent polymer blends. *Adv. Mater.* **14,** 1625–1629 (2002).
9. Kim, S.-J. & Reneker, D. H. A mechanochromic smart material. *Polym. Bull.* **31,** 367–374 (1993).
10. Nallicheri, R. A. & Rubner, M. F. Investigations of the mechanochromic behavior of poly(urethane diacetylene) segmented copolymers. *Macromolecules* **24,** 517–525 (1991).
11. Foulger, S. H. *et al.* Mechanochromic response of poly(ethylene glycol) methacrylate hydrogel encapsulated crystalline colloidal arrays. *Langmuir* **17,** 6023–6026 (2001).
12. Foulger, S. H. *et al.* Photonic crystal composites with reversible high-frequency stop band shifts. *Adv. Mater.* **15,** 685–689 (2003).
13. Comrie, J. E. & Huck, W. T. S. Exploring actuation and mechanotransduction properties of polymer brushes. *Macromol. Rapid Commun.* **29,** 539–546 (2008).
14. Azzaroni, O. *et al.* Mechanically induced generation of counterions inside surface-grafted charged macromolecular films: Towards enhanced mechanotransduction in artificial systems. *Angew. Chem. Int. Edn Engl.* **45,** 7440–7443 (2006).
15. Hickenboth, C. R. *et al.* Biasing reaction pathways with mechanical force. *Nature* **446,** 423–427 (2007).
16. Potisek, S. L. *et al.* Mechanophore-linked addition polymers. *J. Am. Chem. Soc.* **129,** 13808–13809 (2007).
17. Tipikin, D. S. Mechanochromism of organic compounds by the example of spiropyran. *Russ. J. Phys. Chem.* **75,** 1720–1722 (2001).
18. Minkin, V. I. Photo-, thermo-, solvato-, and electrochromic spiroheterocyclic compounds. *Chem. Rev.* **104,** 2751–2776 (2004).

19. Percec, V. *et al.* Ultrafast synthesis of ultrahigh molar mass polymers by metal-catalyzed living radical polymerization of acrylates, methacrylates, and vinyl chloride mediated by SET at 25 degrees C. *J. Am. Chem. Soc.* **128,** 14156–14165 (2006).
20. Casale, A. & Porter, R. S. *Polymer Stress Reactions* Vol. 1, 8–80 and 96–101 (Academic Press, 1978).
21. Ben-Nun, M. & Martinez, T. J. *Ab initio* quantum molecular dynamics. *Adv. Chem. Phys.* **121,** 439–512 (2002).
22. Sotomayor, M. & Schulten, K. Single-molecule experiments *in vitro* and in silico. *Science* **316,** 1144–1148 (2007).
23. Saitta, A. M. & Klein, M. L. First-principles molecular dynamics study of the rupture processes of a bulklike polyethylene knot. *J. Phys. Chem. B* **105,** 6495–6499 (2001).
24. Beyer, M. K. The mechanical strength of a covalent bond calculated by density functional theory. *J. Chem. Phys.* **112,** 7307–7312 (2000).
25. Hiramatsu, Y. & Oka, Y. Determination of the tensile strength of rock by a compression test of an irregular test piece. *Int. J. Rock Mechan. Mining Sci.* **3,** 89–99 (1966).
26. Sternberg, E. & Rosenthal, F. The elastic sphere under concentrated loads. *J. Appl. Mech.* **19,** 413–421 (1952).
27. Eyring, E. Viscosity, plasticity, and diffusion as examples of absolute reaction rates. *J. Chem. Phys.* **4,** 283–291 (1936).

Supplementary Information is linked to the online version of the paper at www.nature.com/nature.

Acknowledgements We acknowledge the support of the ARO MURI programme (grant number W911NF-07-1-0409) for this research.

Author Information Reprints and permissions information is available at www.nature.com/reprints. Correspondence and requests for materials should be addressed to N.R.S. (n-sottos@illinois.edu).